

Surface and Optical Properties of Gd-Doped ZrO₂ Nano Films [†]

Ognian Dimitrov ^{1,*}, Irina Stambolova ², Sasho Vassilev ¹, Katerina Lazarova ³ and Silvia Simeonova ⁴

¹ Institute of Electrochemistry and Energy Systems, Bulgarian Academy of Sciences, Akad. G. Bonchev str, bl. 10, Sofia 1040, Bulgaria; sasho.vassilev@iees.bas.bg

² Institute of General and Inorganic Chemistry, Bulgarian Academy of Sciences, Akad. G. Bonchev str, bl. 11, Sofia 1040, Bulgaria; stambolova@yahoo.com

³ Institute of Optical Materials and Technologies, Bulgarian Academy of Sciences, Akad. G. Bonchev str, bl. 109, Sofia 1040, Bulgaria; klazarova@iomt.bas.bg

⁴ Faculty of Chemistry and Pharmacy, Sofia University, 1 James Bourchier blvd, Sofia 1040, Bulgaria; fhsss@chem.uni-sofia.bg

* Correspondence: ognian.dimitrov@iees.bas.bg

† Presented at the 2nd International Online-Conference on Nanomaterials, 15–30 November 2020; Available online: <https://iocn2020.sciforum.net/>.

Published: 15 November 2020

Abstract: Nanosized coatings of ZrO₂ were deposited on silicon substrates using sol-gel and spin coating techniques. The precursor solutions were prepared from ZrOCl₂·8H₂O with the addition of different percentage (0.5–5%) of rare earth Gd³⁺ ions as dopant. The thin films were homogeneous, with average thickness of 115 nm and refractive index (n) of 1.83. The X-ray diffraction analysis (XRD) revealed the presence of a varying mixture of monoclinic and tetragonal ZrO₂ polycrystalline phases, depending on the dopant, all of which with nanosized crystallites. Scanning electron microscopy (SEM) as well as atomic force microscopy (AFM) methods were deployed to investigate the surface morphology and roughness of the thin films, respectively. They revealed a smooth, well uniform and crack-free surface with average roughness of 0.8 nm. It was established that the dopant concentration affects the photoluminescence (PL) properties of the samples. The undoped films exhibited broad violet-blue PL emission, while the addition of Gd³⁺ ions resulted in new narrow bands in both UV-B and visible light regions, characteristic of the rare earth metal. The intensive emission located at 313 nm can find useful application in medical lamps for treatment of different skin conditions.

Keywords: zirconium dioxide; spin coating; rare earth metal; photoluminescence

1. Introduction

Zirconium dioxide thin films have been investigated for a long time as nano coatings suitable for wear resistance and corrosion protection layers, sensors and bio implants due to their thermal and chemical stability, high hardness, corrosion resistance and biocompatibility [1–4]. Recently they attract attention as candidates for applications in the optical fields as well because of their high refractive index, large optical band gap, low optical loss and high transparency in the visible and near infrared region [5]. The Zr⁴⁺ ion itself do not exhibit photoluminescence properties, but this could be affected strongly by the local defects. Typically, they include different types of impurities, oxygen vacancies, free radicals, etc. that can facilitate broad band PL emission [6]. The sol-gel deposition technique is known to promote the formation of these types of defects in the thin films. Another approach to activate the PL emission is incorporation of luminescent materials, including transition

metals and lanthanide ions into the host lattice of ZrO₂. The low-phonon energy of ZrO₂ opens up the possibility of more efficient luminescence from the activator ions incorporated in it [7]. This is due to the fact that the lower the phonon energy of the host, the higher the probability of radiative transitions of rare earth 3+ ions [8]. In the present work, we incorporated different amounts of Gd³⁺ ions in sol-gel deposited ZrO₂ thin films and monitored the changes in the PL emission as well as the surface morphology, optical properties and phase composition of the films.

2. Materials and Methods

The different sols used for spin coating deposition of the ZrO₂ nano films were prepared using ZrOCl₂·8H₂O which was dissolved in ethanol under vigorous stirring. The zirconium concentration was fixed to 0.25M in all of them. Small amounts of HNO₃ and acetyl acetone were also added to serve as catalyst and complexing agent respectively in molar ratios as follows: ZrOCl₂:HNO₃:AcAc = 6:1:1. The source of Gd³⁺ ions used as a doping agent was Gd(NO₃)₃·6H₂O which was added in different concentrations to form four new precursor solutions: with 0.5, 1, 2 and 5% Gd with respect to the zirconium.

The sol-gel deposition was carried out with a commercial spin coating apparatus (Ossila Spin Coater L2001A3) on silicon substrates, which were cleaned previously in ethanol. The deposition program was set to 5000 rpm with spinning duration of 3 s. After each layer the films were dried at 150 °C for 10 min in air and then annealed at 600 °C for 1 h in air to achieve better crystallinity. This procedure was repeated three times until the films thickness reached about 115 nm.

The phase composition of the samples was studied by X-ray diffraction with CuK α -radiation (Philips PW 1050 apparatus). The size of crystallites was calculated using Scherrer's formula. A scanning electron microscope (JEOL JEM-200CX) was used for morphology observation of the films. The images were taken in secondary electrons mode (SE) at accelerating voltage of 80 keV. The surface topography of the samples was studied with NanoScopeV atomic force microscope (Bruker Inc.), operating in a tapping mode in air. The scanning rate was set at 1 Hz and all images were subsequently smoothed by means of the Nanoscope software. The optical reflectance spectra of the samples were measured using UV-VIS-NIR spectrophotometer Cary 5E (Varian) in the spectral range 320–800 nm. The photoluminescence measurements were performed at room temperature at an excitation wavelength of 230 nm by a FluoroLog3–22 Spectrofluorometer (Horiba Jobin Yvon).

3. Results and Discussion

3.1. Phase Structure

The investigation of the phase structure of the films was carried out with XRD analyses and it revealed that all samples possess a mixture of tetragonal (PDF 88–1007) and monoclinic (PDF 37–1484) ZrO₂ crystallographic phases (Figure 1). The formation of these phases usually depend on the annealing temperature (T_{ann}) used for crystallization: monoclinic structure forms at $T_{\text{ann}} < 1170$ °C, while tetragonal structure stabilizes at T_{ann} between 1170 and 2370 °C [9]. In our case, the addition of Gd resulted in preferential stabilization of the tetragonal phase at lower temperature ($T_{\text{ann}} = 600$ °C). This however is not an unusual phenomenon when rare earth metals are used as dopants in sol-gel produced ZrO₂ [9]. It is also observed that the crystallites associated with the main 101 tetragonal peak on the 2% Gd sample have decreased in size with 1/3 compared to the undoped ZrO₂ film.

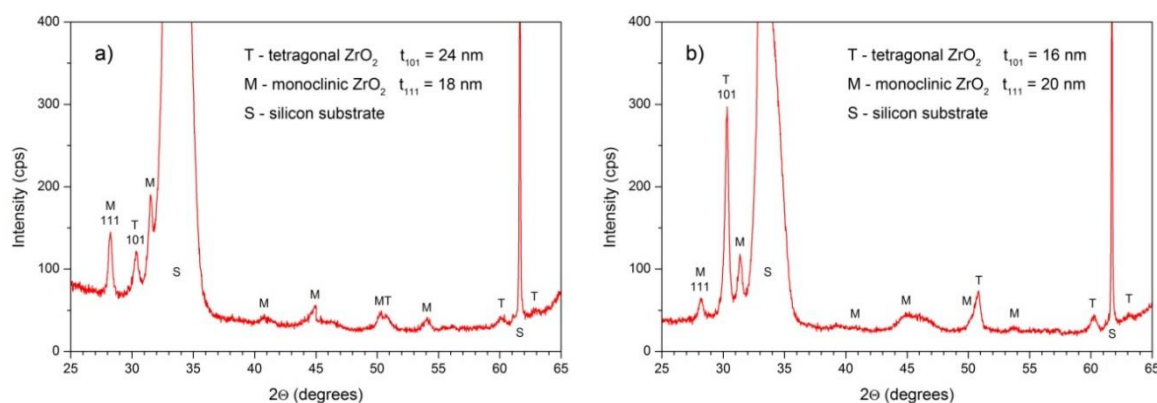


Figure 1. X-ray diffractograms of undoped ZrO₂ thin film (a) and thin film doped with 2% Gd (b).

3.2. Surface Morphology

In order to investigate the surface morphology of the thin films, SEM and AFM techniques were deployed. Figure 2 depicts SEM images at 10,000 and 100,000 magnifications of doped and undoped ZrO₂ coatings. No difference can be seen between the two samples—both films possess very smooth, homogeneous and crack free surface.

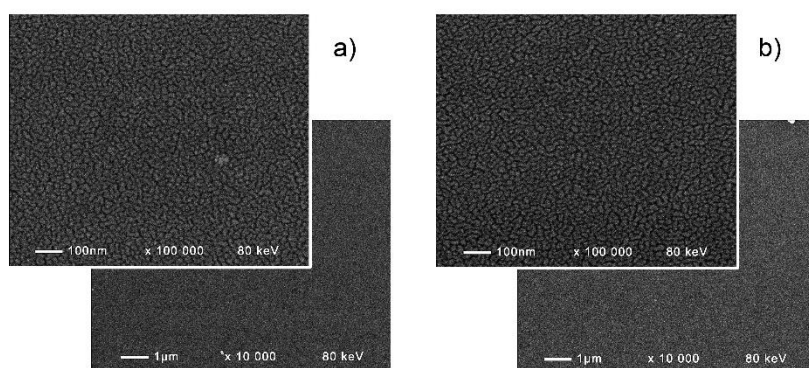


Figure 2. SEM images of undoped ZrO₂ thin film (a) and thin film doped with 2% Gd (b).

Similar observations can be made from the AFM images on Figure 3. At low concentration, the dopant doesn't change the fine, uniform morphology of the thin films surface. At 5% Gd however, slight changes are present: the underlaying of the film becomes smoother on the account of secondary particles being formed on the surface. There is also a slight increase of roughness with the increase of dopant concentration, while the average roughness of the films is about 0.8 nm (Table 1).

Table 1. Root-mean-square roughness (nm) of the thin films surface as measured by AFM analyses.

	Undoped ZrO ₂	Gd 1%	Gd 5%
Rq at 2 μm measurement	0.702	0.819	0.910
Rq at 5 μm measurement	0.618	0.856	0.940

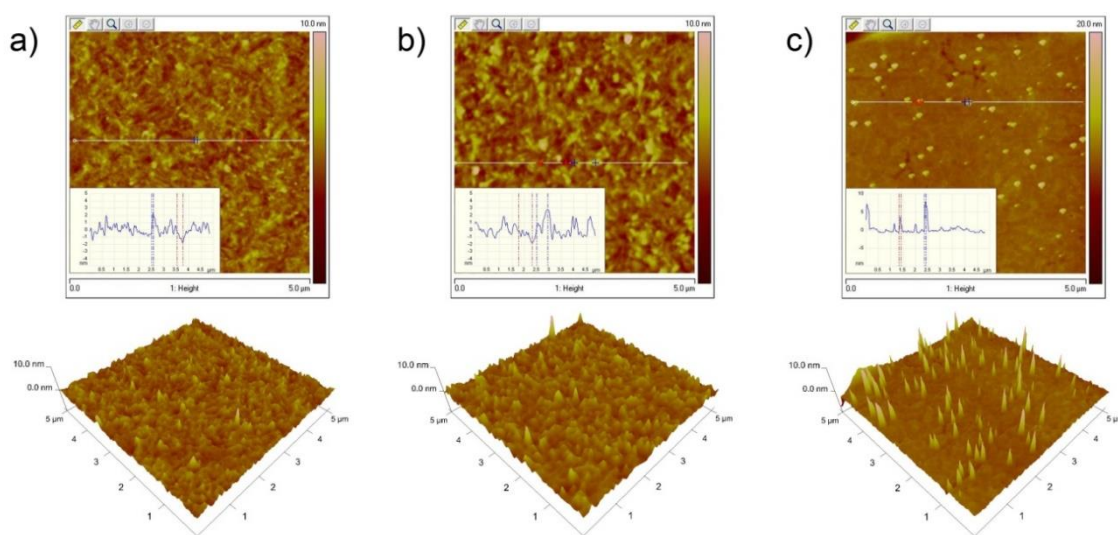


Figure 3. AFM images of undoped ZrO₂ thin film (a) and thin films doped with 1% (b) and 5% Gd (c).

3.3. Optical Properties

The optical reflectance spectra of the samples were measured at normal light incidence. The optical constants (n and k) and the films thickness were determined from the reflectance spectra of the films using previously developed calculating procedure [10]. All films dispersion curves obeyed normal dispersion. The data for the refractive index and the extinction coefficient is taken at wavelengths of 600 nm. A summary of the thickness and optical constants for the whole series of thin films is presented in Table 2.

Table 2. Thickness (nm), refractive index and extinction coefficient of the thin films.

% of Gd	Thickness	n	k
Undoped	106.3	1.83	0.004
0.5%	104.3	1.84	0.006
1%	106.9	1.84	0.003
2%	125.0	1.81	0.002
5%	136.1	1.63	0.013

The photoluminescence spectra of the samples were obtained in the wavelength range of 245–800 nm with excitation radiation of 230 nm (5.39 eV). The PL emission consisted of two distinctive narrow peaks in the UV-B and red regions and one broad band between them, centered at about 425 nm (Figure 4a). Lin et al. reported that tetragonal ZrO₂ nanocrystalline powders showed whitish blue emission at 425 nm owing to some carbon defects [11]. Indeed, the existence of these defects may lead to charge imbalances in local regions of the crystal structure that could be eliminated by the recombination of holes and electrons, facilitating the PL emission. These carbon defects could have been introduced in our thin films via the sol-gel precursors. The two other peaks in the PL spectra are due to the rare earth metal ions as they appear only in the doped films. The UV-B band at 313 nm is very typical of the Gd³⁺ ions and it's related to transitions corresponding to the ⁶P_{7/2} → ⁸S_{7/2} energy states [12] as depicted on Figure 4b. This type of radiation is known to be effective for treating skin diseases such as vitiligo vulgaris, psoriasis, and periodontitis [13–18].

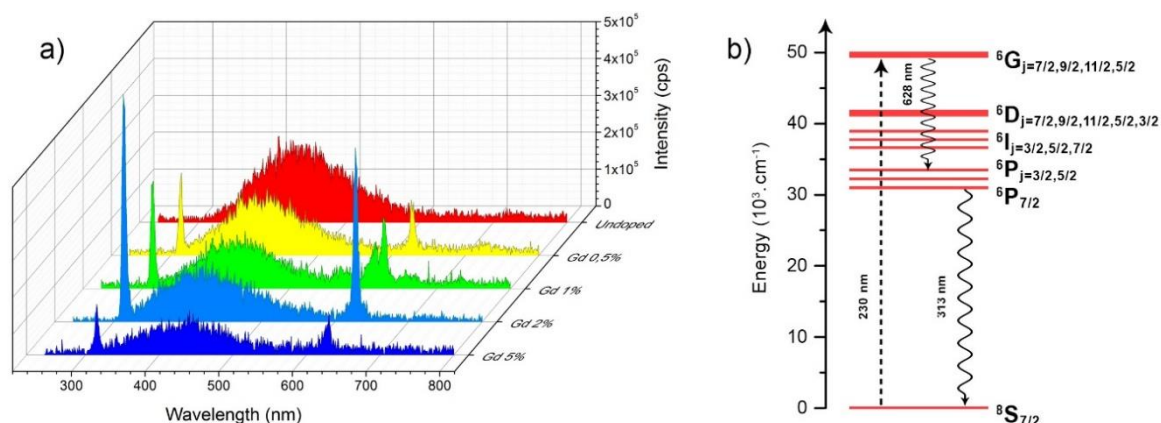


Figure 4. PL emission spectra of the films (a) and energy levels diagram of Gd³⁺ transitions (b).

The red emission peak at 628 nm can be attributed to the ${}^6G_{7/2} \rightarrow {}^6P_{3/2}$ transition as the excitation energy of 5.39 eV should be enough for the excited electron to reach the conduction band of the host material where the 6G_j energy state of Gd³⁺ is located [19]. The overall emission colour of our thin films is pinpointed on the CIE chromaticity diagram shown in Figure 5a. It is observed that the dopant addition results in a slight red shift from the light blue of the pure ZrO₂ film towards more violet colours. It has been established that the optimal dopant concentration that gives the highest intensity of UV-B and red emission in our experiment is 2% Gd. At 5% the quenching effect already takes hold and the intensity of the PL emission decreases (Figure 5b).

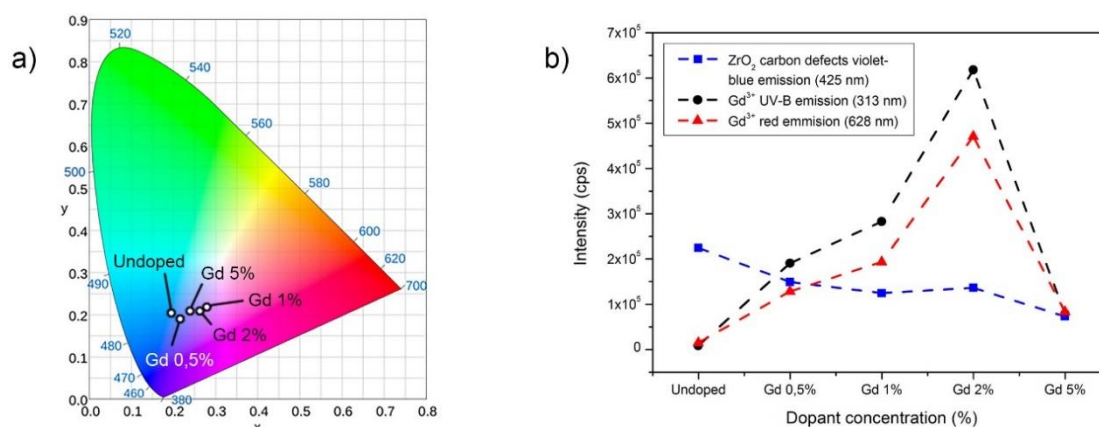


Figure 5. CIE chromaticity diagram with colour coordinates for each sample (a) and evolution of the main emission peaks with dopant concentration (b).

4. Conclusions

A series of thin, homogeneous films of ZrO₂, doped with different amounts of Gd (0.5–5%) were successfully deposited by spin coating technique. The phase structure analyses revealed the presence of both tetragonal and monoclinic ZrO₂ crystallographic phases. It was established that the rare earth dopant promoted the stabilization of the tetragonal phase as well as the decrease of the crystallites size with one third. The surface morphology of the thin films was very smooth (average roughness of 0.8 nm), without visible cracks and with no great alterations from the presence of the dopant. The refractive index of the films remained high (about 1.83) for the most part of the series. Upon excitation with 230 nm radiation, the samples exhibited violet-blue PL emission. It was established that the rare earth dopant led to a red shift in the films emission. The UV-B band at 313 nm caused by the ${}^6P_{7/2} \rightarrow {}^8S_{7/2}$ energy transition of the Gd³⁺ ion has potential application in phototherapeutic devices for treatment of different skin conditions. The maximum PL intensity in this series of ZrO₂ thin films was found to be at 2% concentration of Gd.

Author Contributions: conceptualization, O.D. and I.S.; methodology, O.D., I.S. and K.L.; validation, I.S., K.L., S.V. and S.S.; investigation, O.D., S.V., K.L. and S.S.; writing—original draft preparation, O.D.; writing—review and editing, I.S., K.L., S.V. and S.S.; visualization, O.D.; supervision, I.S. All authors have read and agreed to the published version of the manuscript.

Funding: This research received no external funding.

Acknowledgments: Research equipment of distributed research infrastructure INFRAMAT (part of Bulgarian National roadmap for research infrastructures) supported by Bulgarian Ministry of Education and Science under contract D01-284/17.12.2019 was used in this investigation.

Conflicts of Interest: The authors declare no conflict of interest.

References

1. Izumi, K.; Minami, N.; Uchida, Y. Sol-Gel-Derived Coatings on Steel Sheets. *Key Eng. Mater.* **1998**, *150*, 77–88, doi:10.4028/www.scientific.net/kem.150.77.
2. Zhang, Z.; Ji, G.; Shi, Z. Tribological properties of ZrO₂ nanofilms coated on stainless steel in a 5% NaCl solution, distilled water and a dry environment. *Surf. Coat. Technol.* **2018**, *350*, 128–135, doi:10.1016/j.surfcoat.2018.07.028.
3. Dankeaw, A.; Pongchan, G.; Panapoy, M.; Ksapabutr, B. In-situ one-step method for fabricating three-dimensional grass-like carbon-doped ZrO₂ films for room temperature alcohol and acetone sensors. *Sensors Actuators B Chem.* **2017**, *242*, 202–214, doi:10.1016/j.snb.2016.11.055.
4. Kalaraj, G.S.; Vishwakarma, V.; Kirubakaran, K.; Dharini, T.; Muthaiah, B. Corrosion and biocompatibility behaviour of zirconia coating by EBPVD for biomedical applications. *Surf. Coat. Technol.* **2018**, *334*, 336–343, doi:10.1016/j.surfcoat.2017.11.047.
5. Berlin, I.J.; Lekshmy, S.S.; Ganesan, V.; Thomas, P.V.; Joy, K. Effect of Mn doping on the structural and optical properties of ZrO₂ thin films prepared by sol–gel method. *Thin Solid Films* **2014**, *550*, 199–205, doi:10.1016/j.tsf.2013.10.164.
6. Lakshmi, J.S.; Berlin, I.J.; Daniel, G.P.; Thomas, V.P.; Joy, K. Effect of calcination atmosphere on photoluminescence properties of nanocrystalline ZrO₂ thin films prepared by sol–gel dip coating method. *Phys. B* **2011**, *406*, 3050–3055, doi:10.1016/j.physb.2011.05.004.
7. Salas, P.; Angeles-Chavez, C.; Montoya, J.A.; De la Rosa, E.; Diaz-Torres, L.A.; Martinez, A.; Romero-Romo, M.A.; Morales, J. Synthesis, characterization and luminescence properties of ZrO₂:Yb³⁺-Er³⁺ nanophosphor. *Opt. Mater.* **2005**, *27*, 1295–1300, doi:10.1016/j.optmat.2004.10.019.
8. Lovisa, L.X.; Araújo, V.D.; Tranquilin, R.L.; Longo, E.; Li, M.S.; Paskocimas, C.A.; Bomio, M.R.D.; Motta, F.V. White photoluminescence emission from ZrO₂ co-doped with Eu³⁺, Tb³⁺ and Tm³⁺. *J. Alloys Comp.* **2016**, *674*, 245–251, doi:10.1016/j.jallcom.2016.03.037.
9. Córdova-Martínez, W.; De la Rosa-Cruz, E.; Díaz-Torres, L.A.; Salas, P.; Montoya, A.; Avendaño, M.; Rodríguez, R.A.; Barbosa-García, O. Nanocrystalline tetragonal zirconium oxide stabilization at low temperatures by using rare earth ions: Sm³⁺ and Tb³⁺. *Opt. Mater.* **2002**, *20*, 263–271, doi:10.1016/S0925-3467(02)00067-8.
10. Lazarova, K.; Vasileva, M.; Marinov, G.; Babeva, T. Optical characterization of sol–gel derived Nb₂O₅ thin films. *Opt. Laser Technol.* **2014**, *58*, 114–118, doi:10.1016/j.optlastec.2013.11.014.
11. Lin, C.K.; Zhang, C.M.; Lin, J. Phase transformation and photoluminescence properties of nanocrystalline ZrO₂ powders prepared via the Pechini-type sol-gel process. *J. Phys. Chem. C* **2007**, *111*, 3300–3307, doi:10.1021/jp066615l.
12. Zhong, J.; Liang, H.; Su, Q.; Zhou, J.; Huang, Y.; Gao, Z.; Tao, Y.; Wang, J. Luminescence properties of NaGd(PO₃)₄:Eu³⁺ and energy transfer from Gd³⁺ to Eu³⁺. *Appl. Phys. B* **2010**, *98*, 139–147, doi:10.1007/s00340-009-3673-y.
13. Tjioe, M.; Gerritsen, M.J.P.; Juhlin, L.; Van De Kerkhof, P.C.M. Treatment of vitiligo vulgaris with narrow band UV-B (311 nm) for one year and the effect of addition of folic acid and vitamin B12. *Acta Derm. Venereol.* **2002**, *82*, 369–372, doi:10.1080/000155502320624113.
14. Höningsmann, H. Phototherapy for psoriasis. *Clin. Exp. Dermatol.* **2001**, *26*, 343–350, doi:10.1046/j.1365-2230.2001.00828.x.
15. Reich, A.; Mędrek, K. Effects of narrow band UVB (311 nm) irradiation on epidermal cells. *Int. J. Mol. Sci.* **2013**, *14*, 8456–8466, doi:10.3390/ijms14048456.

16. Takada, A.; Matsushita, K.; Horioka, S.; Furuichi, Y.; Sumi, Y. Bactericidal effects of 310 nm ultraviolet light-emitting diode irradiation on oral bacteria. *BMC Oral Health* **2017**, *17*, 96, doi:10.1186/s12903-017-0382-5.
17. Berneburg, M.; Röcken, M.; Benedix, F. Phototherapy with narrowband vs broadband UVB. *Acta Derm. Venereol.* **2005**, *85*, 98–108, doi:10.1080/00015550510025579.
18. Tamboli, S.; Nair, G.B.; Dhoble, S.J.; Burghate, D.K. Energy transfer from Pr³⁺ to Gd³⁺ ions in BaB₈O₁₃ phosphor for phototherapy lamps. *Phys. B* **2018**, *535*, 232–236, doi:10.1016/j.physb.2017.07.042.
19. Motlounge, S.V.; Motaung, T.E.; Hlatshwayo, T.T.; Koao, L.F.; Malevu, T.D.; Mpelane, S. Associated aspects on structure, morphology and photoluminescence of MgAl₂O₄:x% Gd³⁺ nanophosphor prepared via citrate sol-gel method. *J. Electron. Mater.* **2019**, *48*, 3947–3957, doi:10.1007/s11664-019-07157-y.

Publisher's Note: MDPI stays neutral with regard to jurisdictional claims in published maps and institutional affiliations.



© 2020 by the authors. Submitted for possible open access publication under the terms and conditions of the Creative Commons Attribution (CC BY) license (<http://creativecommons.org/licenses/by/4.0/>).